ACS OMEGA

http://pubs.acs.org/journal/acsodf

Article

Facile Synthesis of Pure and Cr-Doped WO_3 Thin Films for the Detection of Xylene at Room Temperature

Srinivasa Rao Sriram, Saidi Reddy Parne,* Nagaraju Pothukanuri,* Dhananjay Joshi, and Damodar Reddy Edla

Cite This: *ACS Omega* 2022, 7, 47796−47805

Read Online

ACCESS | Metrics & More | Article Recommendations

ABSTRACT: This paper focused on the preparation of pure and Cr-doped tungsten trioxide (WO_3) thin films using the spray pyrolysis method. Different techniques were adopted to analyze these films' structural and morphological properties. The X-ray detection analysis showed that the average crystallite size of the WO_3-nanostructured thin films increased as the Cr doping concentration increased. The atomic force microscopy results showed that the root-mean-square roughness of the films increased with Cr doping concentration up to 3 wt % and then decreased. The increased roughness is favorable for gas-sensing applications. Surface morphology and elemental analysis of the films were studied by field emission scanning electron microscopy with energy-dispersive X-ray spectroscopy measurements. The 3 wt % Cr-WO_3 has a large nanoflake-like structure with high surface roughness and porous morphology. Gas-sensing characteristics of undoped and Cr-doped WO_3 thin films were investigated with various gases at room temperature. The results showed that 3 wt % Cr-doped WO_3 film performed the maximum response toward 50 ppm of xylene with excellent selectivity at room temperature. We believe that increased lattice defects, surface morphology, and roughness due to Cr doping in the WO_3 crystal matrix might be responsible for increased xylene sensitivity.

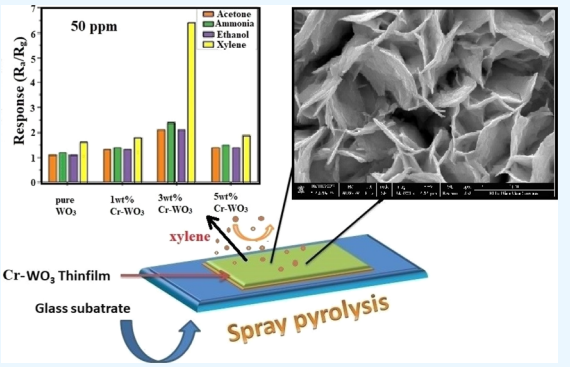

1. INTRODUCTION

Gas sensing technology is quickly evolving in fields such as air quality monitoring,[1,2] electronic nose,[3,4] food quality,[5,6] and medical diagnostics.[7] Manufacturing gas sensors is one of the most rapidly expanding research areas. In gas sensors, the sensing material plays an essential function. Nowadays, toxic and combustible gases are commonly released from industries and vehicles into the environment, leading to air pollution and a serious hazard to human health and living organisms. Highly toxic, flammable, and combustible gases such as carbon monoxide, carbon dioxide, ammonia, hydrogen sulfide, nitrogen oxides, benzene, toluene, and xylene pollute the environment drastically. Among them, xylenes are aromatic hydrocarbons with an undistilled mixture of the three isomers, often used as a solvent in industrial and medical fields. It is a colorless, sweet-smelling gas. Xylene is a solvent used in the paint, printing, rubber, and leather industries. Xylene can also be used as a domestic cleaning agent. The National Institute for Occupational Safety and Health proposed xylene exposure limits of 100 ppm for 10 min. Exposure to xylene may happen through inhalation, ingestion, or contact with the eye or skin. Inhaling xylene vapors causes central nervous system disturbance, resulting in symptoms such as headache, fatigue, stomach pain, and vomiting. Long-term exposure can cause hypertension, frustration, sadness, sleeplessness, anxiety, excessive weariness, shaking, poor focus, and short-term memory loss. Therefore, the detection of xylene in the environment is a challenging task for researchers across the globe.

Metal oxides are commonly used as a sensing layer because of their low cost, versatility, and ease of production. Several metal oxides are available, including ZnO, WO_3, In_2O_3, V_2O_5, and TiO_2.[8] WO_3 is an important n-type semiconductor with excellent sensing characteristics, a simple reaction, ease of preparation, adaptability, and other distinctive properties that are important in gas sensing applications. Nanostructured WO_3 shows various structural properties, phase transitions, a high band gap, and a large surface area. These distinct features grabbed the researchers' attention, and prompted them to investigate the gas-sensing properties. WO_3 shows various structural properties and phase transitions at different

Received: August 30, 2022
Accepted: November 24, 2022
Published: December 14, 2022

https://doi.org/10.1021/acsomega.2c05589
ACS Omega 2022, 7, 47796−47805

temperatures.[9] As the temperature increases between 300 and 800 °C, the phase transitions in the WO_3 thin films occur sequentially as monoclinic, orthorhombic, and hexagonal phases. The phase transitions of WO_3 significantly influence its electrical properties, making it beneficial in electrochemical gas sensing applications.[10] Hence, WO_3 has been widely researched as a gas sensor material. However, improving the gas-detecting capability of pure WO_3 substances remains challenging.

Recent investigations reported that metal doping in the metal oxide matrix is one of the strategies to enhance the gas-detecting performance compared to a pure substance.[11−14] For example, Varudkar et al. fabricated Al-doped ZnO nanoparticles, which exhibited an excellent response to ammonia detection.[15] Nagaraju et al. prepared Gd-decorated cerium oxide nanostructured thin films for acetone detection at room temperature with fast response and recovery times.[16] Anusha et al. investigated Ag-doped WO_3-based gas sensors synthesized by spray pyrolysis to detect ammonia gas.[17] Wang et al.[18] synthesized WO_3 nanosheets using a hydrothermal synthesis method; after that, ruthenium was loaded on the surface of the nanosheets with solvothermal treatment. The prepared samples were investigated for xylene sensing applications at high operating temperatures (280 °C). Li et al. prepared Au-doped WO_3 nanoparticles with different atomic percentages of silver using the hydrothermal method for xylene detection applications. The 0.30 atomic % of the Au-doped WO_3-based sensor has shown a response of 26.4 toward 5 ppm of xylene at 255 °C.[19] Li et al.[20] reported preparing pure and Cr-doped WO_3 nanofibers with the spin-coating technique for xylene sensing applications. 4 mol % Cr-doped WO_3 showed the highest response toward 100 ppm xylene at an elevated temperature of 255 °C. Zhang and co-workers[21] have investigated hexagonal WO_3 nanosheets with hydrothermal and sol-hydrothermal methods. Nanoparticles prepared with hydrothermal methods have shown a response of 36.27 toward 50 ppm of xylene at an operating temperature of 320 °C. Guo et al.[22] synthesized CuO/WO_3 composite materials by ultrasonic-wet chemical etching and the pyrolysis method for xylene sensing applications. The 3% mass ratio CuO/WO_3 sensor responded to 50 ppm of xylene at 260 °C. After a careful latest literature review, we have noticed that most of the metal oxide-based materials in the bulk form are used as the xylene sensors operating at elevated temperatures. In the present investigations, we have chosen thin film technology, which has numerous advantages over bulk materials, such as its properties being significantly different and being cost-effective. As the thickness of the film is reduced, the surface-to-volume ratio can increase, which will play a crucial role in many technological applications. We can also control the morphology and microstructure of the films during the deposition process. Various deposition techniques are available to deposit metal oxide-based thin films, such as thermal evaporation, pulsed laser deposition, sputtering, spin coating, electron beam evaporation, and spray pyrolysis. Among all these techniques, spray pyrolysis is the most inexpensive, making it superior to other vacuum deposition processes. A small amount of material is required to be coated on the substrate. The deposition process uses metal salts in aqueous solvents to create metal oxides and composite nanomaterials with precisely regulated morphologies and chemical compositions in an open atmosphere.[23] Dalenjan et al.[24] synthesized cobalt-doped WO_3 thin films with different concentrations of the dopant at a substrate temperature of 400 °C and later on annealed them at 500 °C for 1 h. The annealed films were investigated for electrochromic properties by the cyclic voltammetry analysis technique. They have reported that the WO_3 sample doped with 20% cobalt impurity has significant color variation. Acosta et al. investigated pure, molybdenum-, and titanium-doped WO_3 thin films with different dopant concentrations using the pulsed spray pyrolysis technique on FTO substrates. They have reported a significant impact of dopant on structural, morphological, and electrical properties.[25] Upadhyaya et al.[26] studied Cr-doped WO_3 nanosheets using the chemical coprecipitation method for formaldehyde sensing applications at an operating temperature of 200 °C.

In this work, we successfully fabricated pure and Cr-doped WO_3 thin films using cost-effective spray pyrolysis techniques with optimized deposition parameters. To the best of our knowledge and belief, this is the maiden attempt to prepare Cr-doped WO_3 thin films using the spray pyrolysis technique for xylene sensor applications. The Cr-doped WO_3-based material was discovered to have better gas-sensing characteristics in the presence of xylene at room temperature. The 3 wt % Cr-doped WO_3 sensors showed a fast response toward 50 ppm of xylene, strong selectivity, and a rapid response/recovery time. After Cr doping, the increase in surface roughness and morphological changes might be responsible for the improved performance.

2. EXPERIMENTAL SECTION

2.1. Preparation. Analytical Na_2WO_4 $2H_2O$, Sigma-Aldrich, India, and CrN_3O_9 $9H_2O$, Sigma-Aldrich, Spain, with ≥99% purity, were used as starting precursors without further purification. 20 mL of the Na_2WO_4 aqua solution (0.04 M) was slowly added to 20 mL of CrN_3O_9 ethanol solution (0.04 M). The 40 mL solution was stirred using a magnetic stirrer at room temperature. Then, four drops of acetic acid were added to make a clear and transparent solution. The 40 mL solution was used as a precursor for the spray pyrolysis deposition. The precursor solutions with doping concentrations of 1, 3, and 5 wt % of Cr were prepared. These precursor solutions were sprayed on transparent glass substrates at 400 °C. Undoped and Cr-doped WO_3 thin films with different doping concentrations of 1, 3, and 5 wt % were coated by the spray pyrolysis technique. Glass slides are insulating materials generally used as substrates in the thin-film deposition process. As we know, in the gas sensing mechanism, the target gas interacts with the deposited material and electrons flow through the thin film, but electrons always choose a path of minimum resistance. If the deposited material is on a conducting or semiconducting substrate, the electrons will flow through the substrate instead of coating the material. If the substrate is an insulator, then electrons will flow only through the film and not through the substrate. Hence, we cannot record the exact results from the thin films. Before the deposition, glass substrates were cleaned ultrasonically with an acetone solution and then rinsed thoroughly with deionized water. After that, they were dried for around 30 min in the micro-hot air oven to produce a clean surface. The experimental system (Holmarc-India) had optimized deposition parameters such as the distance between the nozzle and the substrate of 28 cm, the solution flow rate of 2 mL/min, the spray time of 10 min, the solution concentration of 0.04 M, and the use of air as a carrier gas. After the deposition process, substrates were allowed to cool down to room temperature. The film's adhesion to the glass substrate was checked with the

https://doi.org/10.1021/acsomega.2c05589
ACS Omega 2022, 7, 47796−47805

Scotch Tape method, which shows excellent adhesion to the substrates.

2.2. Characterization. X-ray diffraction (XRD) was used to analyze the structural properties of pure and Cr-doped WO_3 thin films utilizing a Bruker D8 ADVANCE diffractometer. In this, Cu Kα was used as a radiation source (λ = 0.1541 nm), and 2θ is the Bragg's diffraction angle in the range of 20−60°. The vibrational modes of thin films were investigated using a Raman spectrometer (LAB RAM HR HORIBA France) fitted with a liquid nitrogen-cooled CCD detector and a pulsed laser (Nd:YAG) with a wavelength of 532 nm at room temperature. Field emission scanning electron microscopy (FESEM) characterization together with energy-dispersive X-ray spectroscopy (EDX) analyses were studied using a field emission scanning electron microscope (Quanta 250 FEG) equipped with an energy-dispersive X-ray spectrometer for elemental analysis. An atomic force microscope (Bruker AFM Probes−RTESPA-300, USA) was used to examine the surface roughness of the pure and Cr-doped WO_3 thin films in the tapping mode with 0.5 Hz frequency. The static approach was used to accomplish the gas sensing characteristics, and the gas sensing setup is shown in Figure 1. Humidity will reduce the

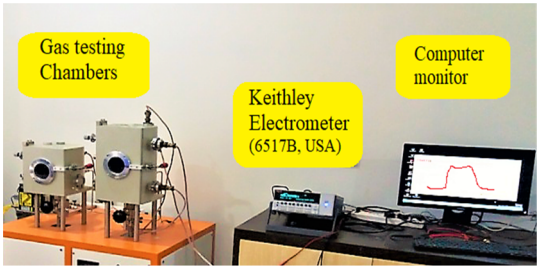

Figure 1. Essential components in the gas testing experiment setup.

sensor's stability; therefore, we have maintained the relative humidity in the chamber at 60% using a digital humidity controller (Humitherm, India) during the gas sensing characterization. The essential components of this arrangement are a gas-detecting chamber, a Keithley electrometer (6517B, USA), and a personal computer.

2.3. Sensor Element Fabrication. After the deposition of pure and Cr-doped WO_3 thin films on glass substrates, these are utilized for gas sensing characterization in the static mode. The films were cut into 2 × 2 cm^2 sizes, and silver paste was printed to provide suitable conductive electrodes and heated for 2 h at 100 °C in a programmable furnace for good electrical contacts. The response of the sensors was estimated by the following equation[27,28]

$$\text{Response of the sensor (S)} = \frac{R_a}{R_g} \quad (1)$$

where R_a = resistance of the sensing layer in the presence of air and R_g = resistance of the sensing layer in the presence of target gas.

3. RESULTS AND DISCUSSION

3.1. XRD Analysis. The thickness of the deposited films is investigated using the weight difference method, and it

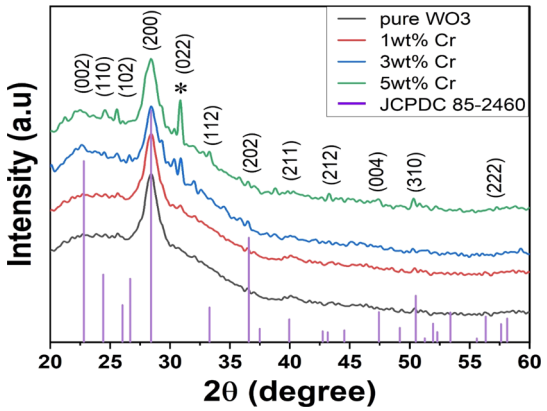

Figure 2. XRD patterns of pure and Cr-doped WO_3 thin films.

increases with increasing Cr doping concentration. The thickness of the deposited thin film is tabulated in Table 1. The crystalline nature of the deposited films has been determined by XRD analysis. Figure 2 shows the XRD pattern of the fabricated pure and Cr-doped WO_3 thin films with various chromium concentrations. The diffraction peaks are attributed to the WO_3 planes of (002), (110), (200), (112), (202), (211), (212), (004), (310), and (222), which corresponded to the recorded values from the JCPDC 85-2460, confirming the hexagonal phase of the deposited thin films. However, a new peak appears in Cr-doped WO_3 films near 30.88°, and the intensity of this peak increases with increasing the Cr concentration. It might be due to the formation of a secondary phase of Cr_2O_3. The following Scherrer formula is used to determine the crystallite size of the deposited thin films[29]

$$\text{Crystallite size} = \frac{0.93 \times \lambda}{\beta \cos\theta} \quad (2)$$

where λ is the wavelength of the X-rays, the λ value is 0.154 nm, θ is the angle of Bragg's diffraction in radian, β is the (FWHM) full width at half maximum of the peak, and calculated crystallite size values are tabulated in Table 1. It was noticed that when the concentration of Cr rose, the average crystal size increased mildly due to the higher tensile stress caused by the doping process. Tensile stress in thin films may be generated due to the change in bond length and differences in local symmetries and microinhomogeneities in the deposited

Table 1. Parameters of the Crystal Structure of Pure and Cr-Doped WO_3 Thin Films

S.No	thin film	average crystallite size (nm)	dislocation density × 10^{-2} (lines/nm^2)	microstrain × 10^{-3}	thickness (nm)
1	pure WO_3	7.50	1.77	4.82	193
2	1 wt % Cr-WO_3	7.59	1.73	4.76	226
3	3 wt % Cr-WO_3	8.25	1.46	4.38	297
4	5 wt % Cr-WO_3	8.41	1.41	4.30	372

https://doi.org/10.1021/acsomega.2c05589
ACS Omega 2022, 7, 47796−47805

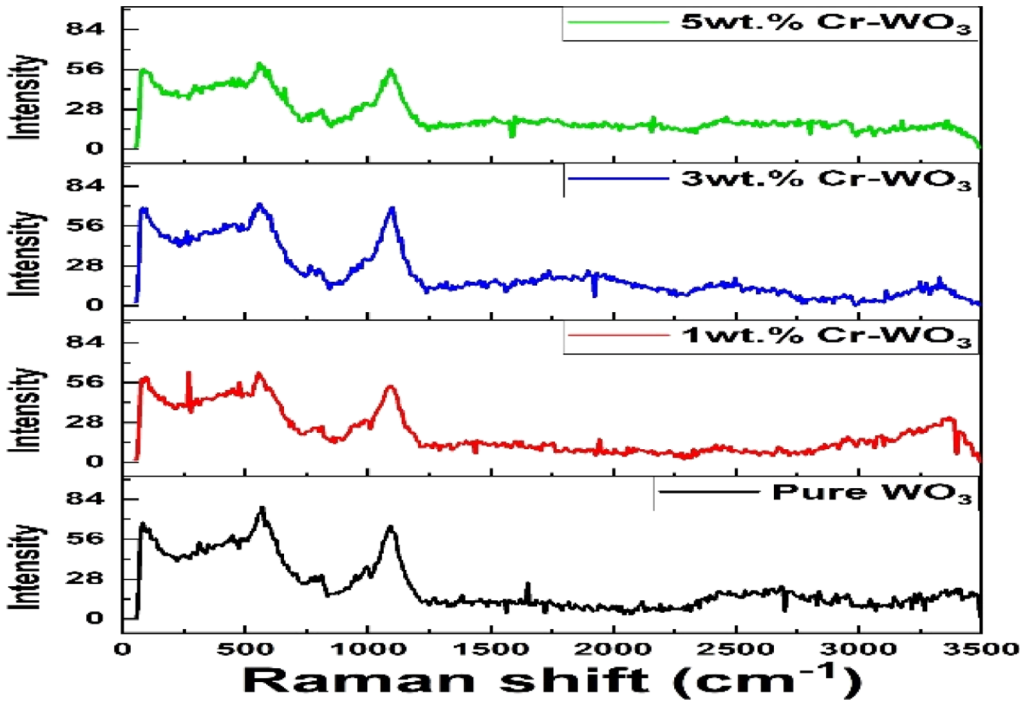

Figure 3. Raman spectra of pure and Cr-doped WO_3 thin films.

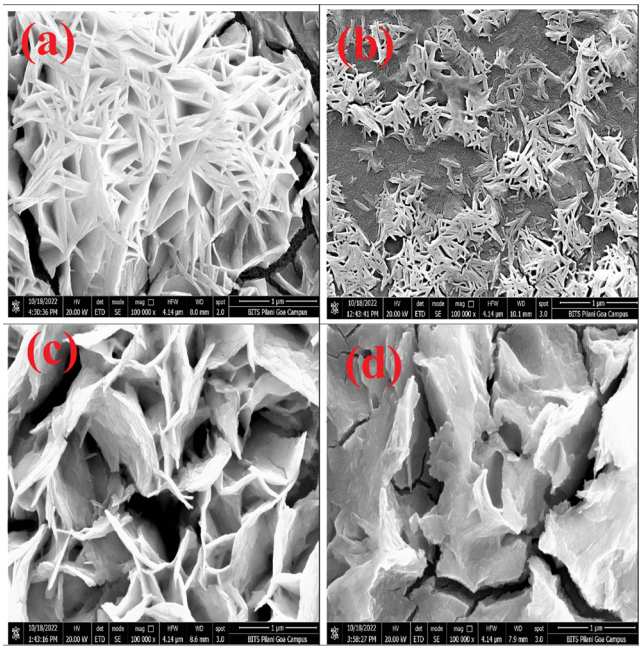

Figure 4. FESEM images of (a) pure WO_3, (b) 1 wt % Cr-doped WO_3, (c) 3 wt % Cr-doped WO_3, and (d) 5 wt % Cr-doped WO_3.

thin films. The material with a large crystalline size and minimum stress is more favorable for gas sensor applications.[30]

The thin films' strain (ε) and dislocation density (δ) are calculated from the formula[31,32]

$$\text{strain } (\varepsilon) = \frac{\beta \cos \theta}{4} \quad (3)$$

$$\text{dislocation density } (\delta) = \frac{1}{(\text{crystallitesize})^2} \quad (4)$$

Calculated strain and dislocation densities are tabulated in Table 1. Strain and dislocation densities are decreased with increasing the doping percentage of chromium atoms in the WO_3 matrix.

3.2. Raman Spectroscopic Analysis. Raman spectroscopy is a specialized instrument for determining a compound's fundamental vibrations and discrepancies. Figure 3 shows the Raman spectra patterns of the pure and Cr-doped WO_3 thin films. It is found from the spectra that the peaks are located at wavenumbers 267, 552, and 807 cm^{-1}. The peaks at 552 and 807 cm^{-1} can be ascribed to the W−O−W bending mode of bridging oxygen, whereas the peak observed at 267 cm^{-1} is attributable to the lattice vibration of crystalline WO_3. A peak at 260 cm^{-1} in the case of 1 wt % Cr-doped WO_3 thin film corresponds to the bending vibrations of O−W−O bridging bonds.[33] The peak widening and peak shifting are found at greater wavenumbers (552 and 807 cm^{-1}), which is attributed to a change in the electronic structure as Cr concentration rises. The Raman spectra intensity is lowered because of stoichiometric deficiencies, quantum confinement effects, crystallinity, and particle size changes.[34] The Raman spectra confirm the substitution of Cr^{3+} ions in the WO_3 lattice site, which is in agreement with X-ray diffraction studies.

3.3. Field Emission Scanning Electron Microscopy. Morphologies of pure WO_3, 1 wt % Cr-WO_3, 3 wt % Cr-WO_3, and 5 wt % Cr-WO_3 were investigated by FESEM, and the images are shown in Figure 4. The SEM images illustrate that the prepared films have an intercrossed, sheet-like morphology. WO_3 nanoparticles can be located at the top/lateral faces of the sheet and makes good contact with each other; also, crystal plane-selective growth parallel to the layer would result in the production of crystalline nanoflakes in the case of the pure thin film, as shown in Figure 4a. However, the nanoflake-like morphology normal to the substrate was observed for both 1 and 3 wt % Cr-doped WO_3 thin films, as shown in Figure 4b,c, respectively. It is also noticed that the height of these

https://doi.org/10.1021/acsomega.2c05589
ACS Omega 2022, 7, 47796−47805

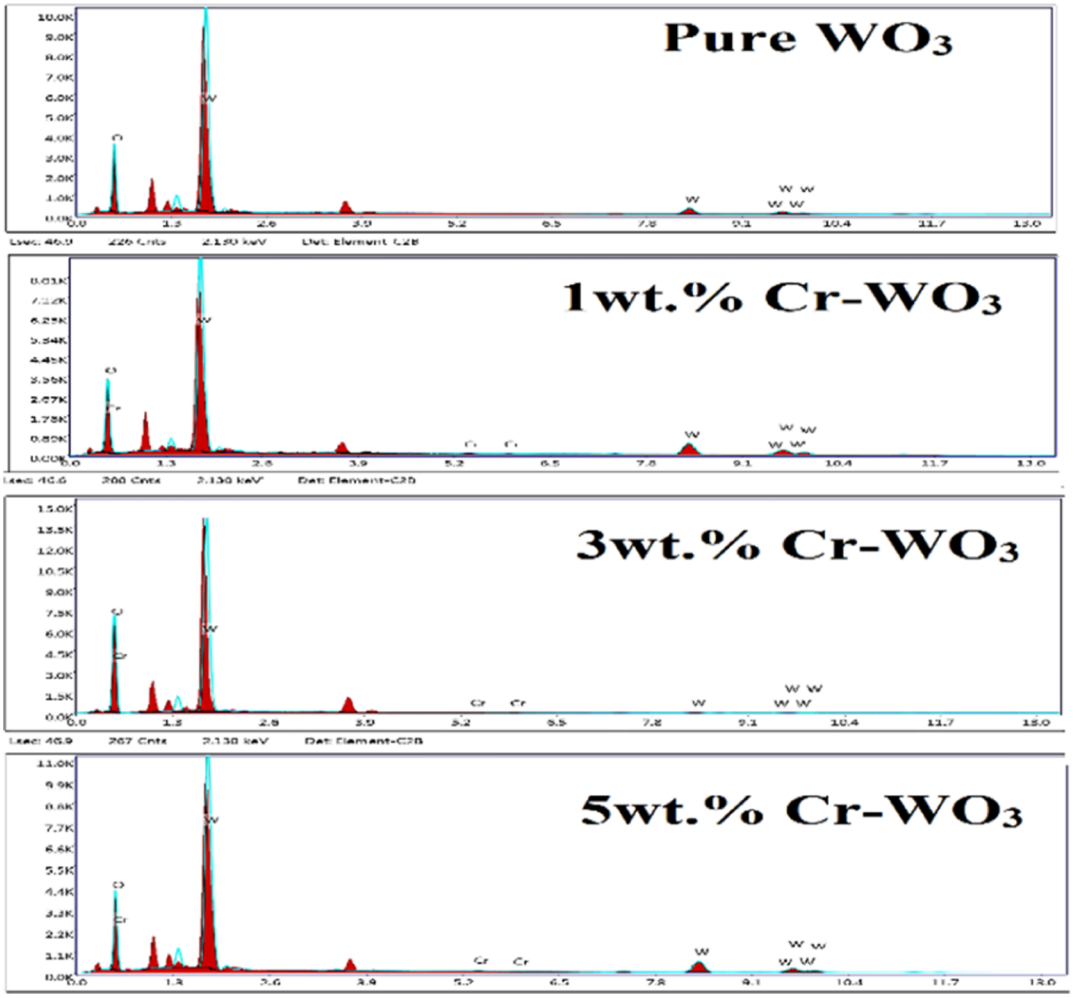

Figure 5. Energy-dispersive X-ray spectroscopy (EDX) spectra of the WO_3-based thin films.

nanoflakes is comparatively large, randomly oriented, and interconnected with high surface roughness and porous morphology in the case of 3 wt % Cr-doped WO_3 thin films compared with other films. Such a kind of nanostructured morphology is helpful in trapping gas molecules that may interact significantly with sensing material and enhance sensor response. At the same time, the flake-like morphology has been reduced in 5 wt % Cr-WO_3 sample with microcracks, as shown in Figure 4d. Elemental analysis has been studied with EDX and the images of pure and Cr-doped WO_3 thin films, as shown in Figure 5. The EDX spectra of pure WO_3 thin film only contain W and O elements. However, in the case of Cr-doped WO_3 thin film spectra, W, O, and Cr elements are clearly seen, confirming the successful incorporation of Cr elements in the WO_3 crystal matrix.

3.4. Atomic Force Microscopy. Atomic force microscopy (AFM) will provide the topography of the films depicted in Figure 6, recorded in the tapping mode of the 1 × 1 μm^2 scan area. The surface features of the films, such as root-mean square (RMS) roughness, kurtosis, and skewness, were determined using Nanoscope E software, and the obtained values are presented in Table 2. The grain height and RMS roughness of the WO_3 films are dependent on the Cr doping process. The obtained values of the roughness of the films formed at various doping concentrations show significant variations. The effective surface area of films with a high roughness value is essential in gas sensor applications. It is observed that the roughness increases first up to 3 wt % Cr-doped WO_3 thin films and then decreases. This is because of the crystal growth rate is slower at 5 wt % Cr doping. Although, greater roughness on the film surface increases the active surface area of interaction for the adsorption of small gas molecules, which is the fundamental property of gas response measurements.[35,36] Skewness is used to explain the symmetry of the changes in a particular plane/line, and this parameter is too sensitive when the plane has deep valleys and high peaks. Negative skewness values show valleys are preponderant on the surface and become more planar. Positive skewness interprets the thin film's lopsided nature and contains more peaks than valleys.[37] Kurtosis (Sku) is sensitive to the sharpness of the peaks. Sku > 3 shows exceptionally sharp features, Sku = 3 indicates a normally distributed surface, and Sku < 3 indicates a more gradually varying surface. The 3 wt % Cr-doped WO_3 film has shown the highest kurtosis and most minor Skewness characteristics. This sample may be more favorable for gas sensing applications.

3.5. Gas Sensing Characteristics. The gas sensing characteristics are determined by the xylene range of 1 to 50 ppm at room temperature. The concentration of xylene gas is measured with the static liquid gas distribution method using the formula.[38] As xylene gas concentrations increase, the sensors' responsiveness increase, and the maximum xylene gas

https://doi.org/10.1021/acsomega.2c05589
ACS Omega 2022, 7, 47796−47805

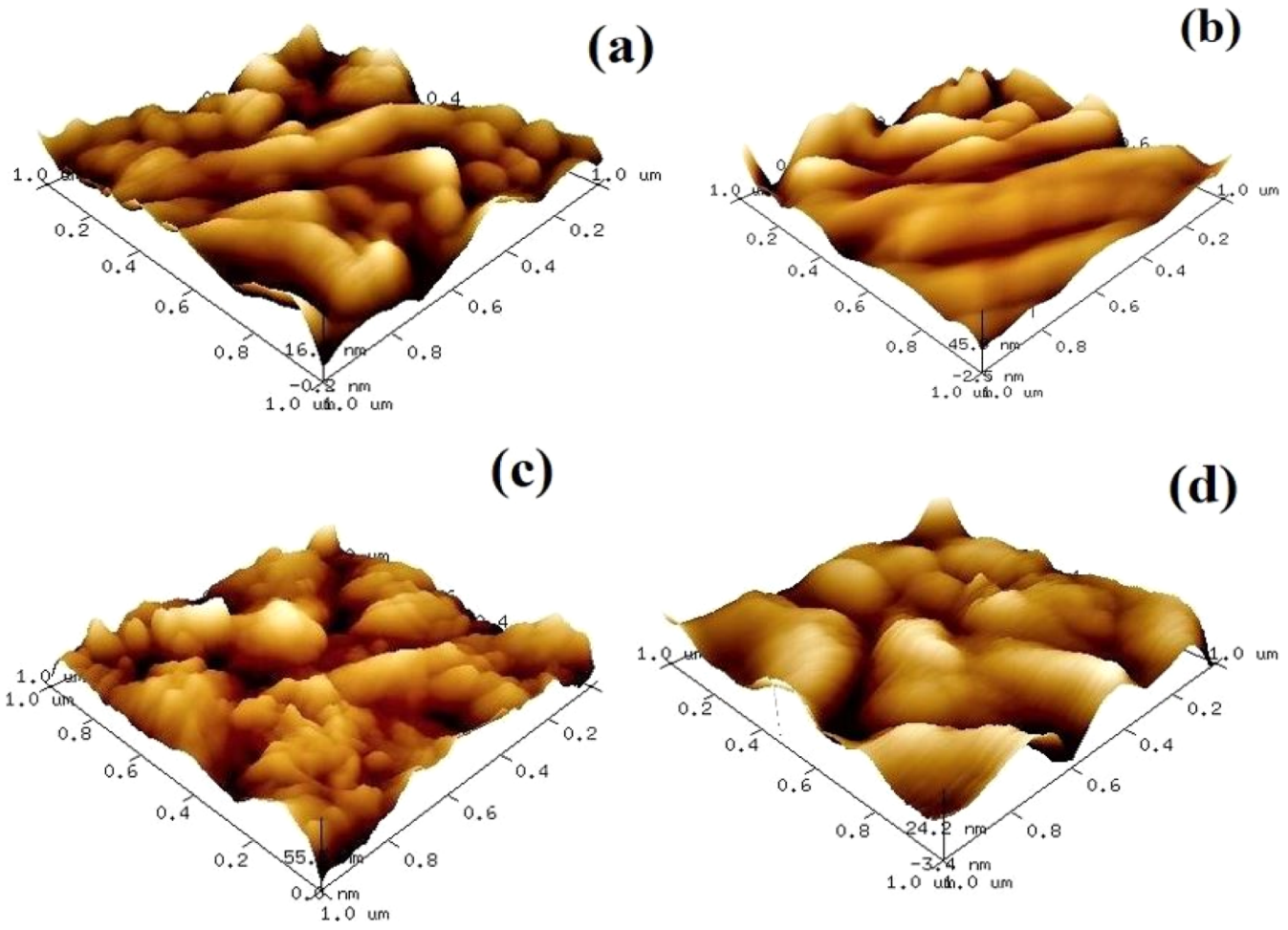

Figure 6. AFM pictures of (a) pure WO_3, (b) 1 wt % Cr-doped WO_3, (c) 3 wt % Cr-doped WO_3, and (d) 5 wt % Cr-doped WO_3.

Table 2. Surface Characteristics of Pure and Various Cr-Doped WO_3 Thin Films

S.No	thin films	RMS roughness (R_q)	average roughness (R_a)	skewness	kurtosis	grain height (nm)
1.	pure WO_3	4.88	3.98	−0.02	2.79	3.68
2.	1 wt % Cr-WO_3	12.9	10.1	−0.12	3.6	13.2
3.	3 wt % Cr-WO_3	15.5	12.4	−0.29	4.21	18.8
4.	5 wt % Cr-WO_3	8.28	6.57	−0.07	3.05	9.2

responses of pure, 1, 3, and 5 wt.% Cr-doped WO_3 are shown in Figure 7. The 3 wt % Cr-doped WO_3-based sensor has a significantly stronger reaction to xylene than the other sensors because of its high roughness, active surface area, and interconnected nanoflake-like morphology.

$$\text{Concentration of test gas } (C_{ppm}) = \frac{22.4 \times V_1 \times D \times \varphi}{V_2 \times M} \quad (5)$$

where D is density (g/mL), V_1 is the volume of the xylene liquid (μL), φ is the volume fraction, M is the molecular wt (g/mol) of xylene, and V_2 is the volume of the chamber (L).

3.5.1. Repeatability and Long-Term Stability. Repeatability can be described as the ability of a sensor to provide the same result under the same working conditions over and over again. At the same time, the long-term stability of a gas sensor is an essential characteristic for carrying out long-term data collection. The ability to maintain a relatively stable and repeatable signal over a sufficient period is defined. The repeatability of the 3 wt % Cr-doped WO_3 film sensor has been exposed to 50 ppm of xylene at room temperature for 1 h, and the sensor has shown stable repeatability during the tenure, as shown in Figure 8a. Long-term stability is depicted in Figure 8b. As a result, the experiment on the long-term stability of a 3 wt % Cr-WO_3 sensor toward 50 ppm of xylene was conducted under ideal circumstances over 1, 5, 10, 15, 20, 25, and 30 days. It is noticed that the response values remain almost the same during the measurements described above. Hence, 3 wt % Cr-doped WO_3 nanoflakes sensors have shown good sensing capabilities which can be used for real-time applications.

3.5.2. Gas Sensing Mechanism. In the presence of air, the oxygen molecules present in the air will adsorb on the film surface and capture the electrons from the conduction band to form O_2^-. When the film is exposed to interact with the xylene, it will react with the oxygen molecules on the surface of the Cr-doped WO_3 film, which leads to a decrease in the oxygen ion concentration on the film surface and an increase in the electron concentration, which leads to a reduction in the resistance of the Cr-doped WO_3 thin film sensor.

https://doi.org/10.1021/acsomega.2c05589
ACS Omega 2022, 7, 47796−47805

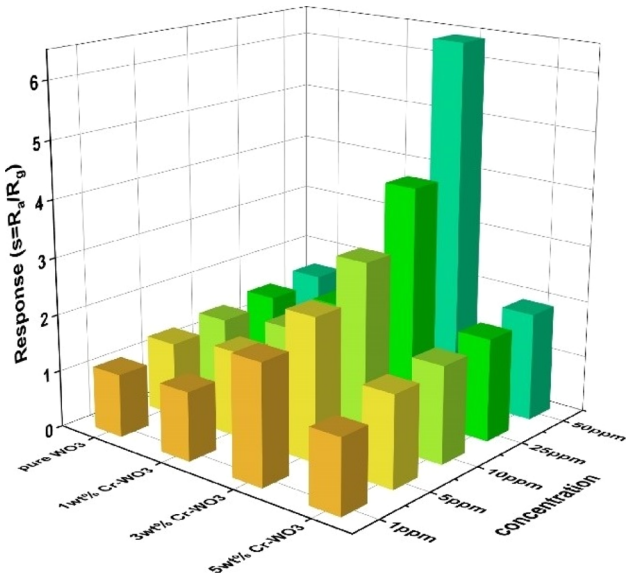

Figure 7. Response of pure and Cr-doped WO_3 films with various concentrations of xylene.

This oxidation of xylene requires the following steps: (a) chemisorption of oxygen in the air followed by the formation of O_2^-, O^-, and O^{2-} ions; (ii) initial enhancement of conductivity owing to an increase in the carrier density and the formation of a conduction layer on the surface; and (iii) chemisorption of xylene (reducing gases) followed by reaction with preadsorbed oxygen. The reaction releases free electrons, resulting in a noticeable decrease in the measured resistance.

$$O_{2(gas)} \rightarrow O_{2(ads)} \quad (6)$$

$$O_{2(ads)} + e^- \rightarrow O_{2(abs)}^{\bullet -} \ (T < 100\ ^\circ C) \quad (7)$$

When the WO_3 thin film is exposed to a xylene gas environment, the xylene gas molecules get adsorbed on the film surface and interact with chemisorbed oxygen species, and some of the xylene gas molecules diffuse into the WO_3 thin film. Since xylene is a reducing gas, it releases electrons onto the sensor surface, increasing the electron carrier concentration of the WO_3-based sensor and thereby decreasing the film sensor's resistance. The magnitude of the change in resistance in this process directly reflects the gas response of the WO_3 thin-film sensor.

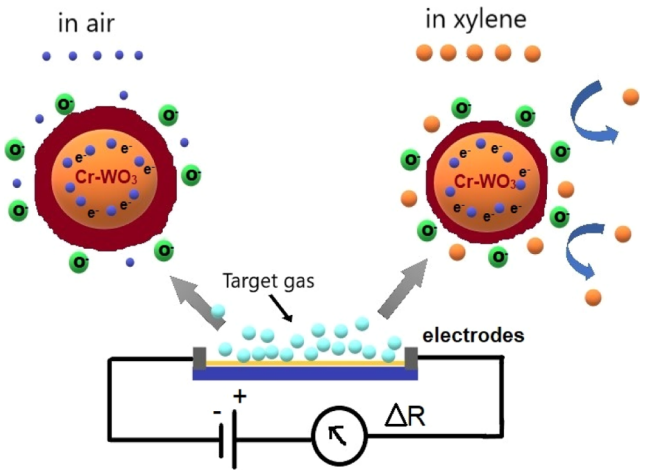

Figure 9. Systematic representation of the sensing mechanism.

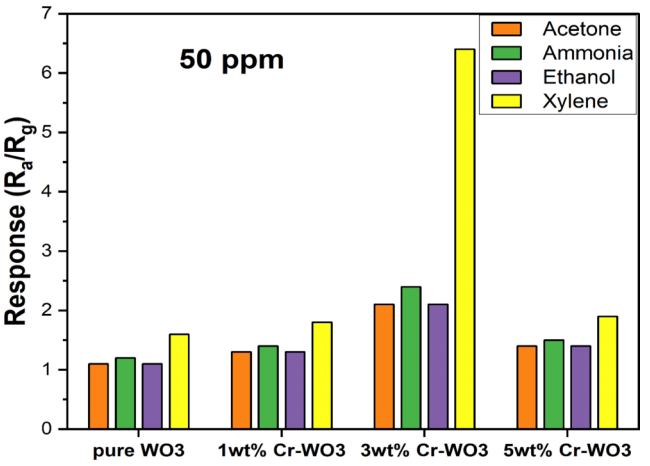

Figure 10. Selectivity of Cr-doped WO_3 films toward certain gases.

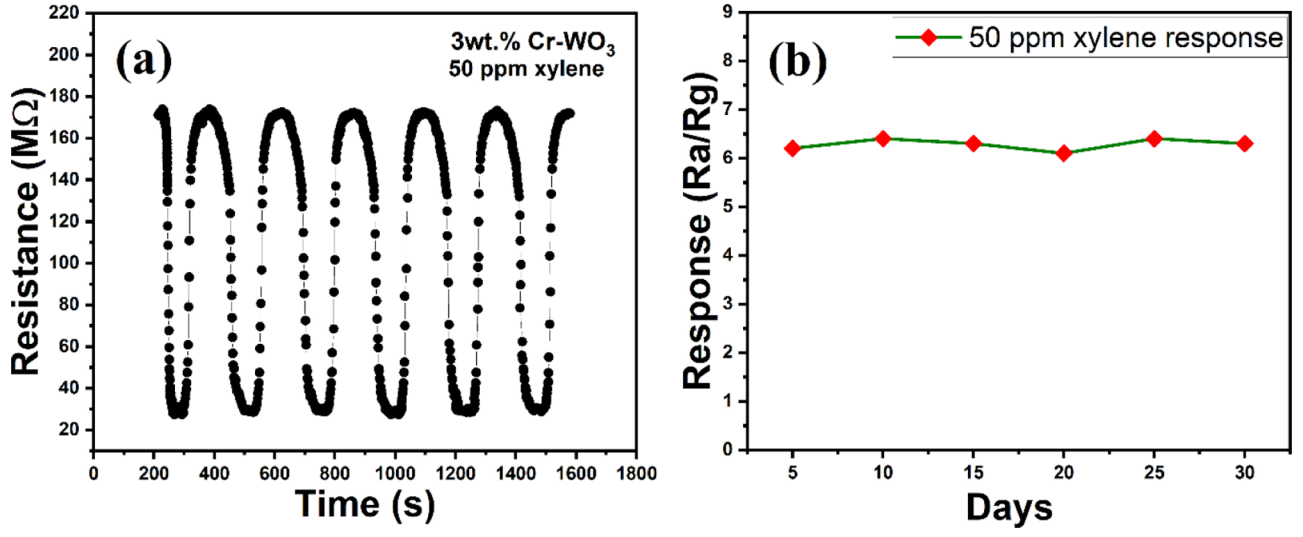

Figure 8. (a) Repeatability and (b) long-term stability for 50 ppm xylene gas of the 3 wt % Cr-WO_3 sensor.

https://doi.org/10.1021/acsomega.2c05589
ACS Omega 2022, 7, 47796−47805

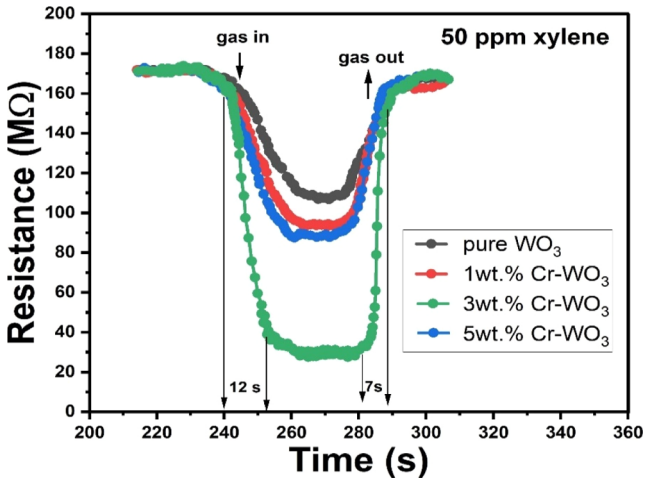

Figure 11. Transient response curve of the 3 wt % Cr-doped WO_3-based sensor response toward 50 ppm of xylene.

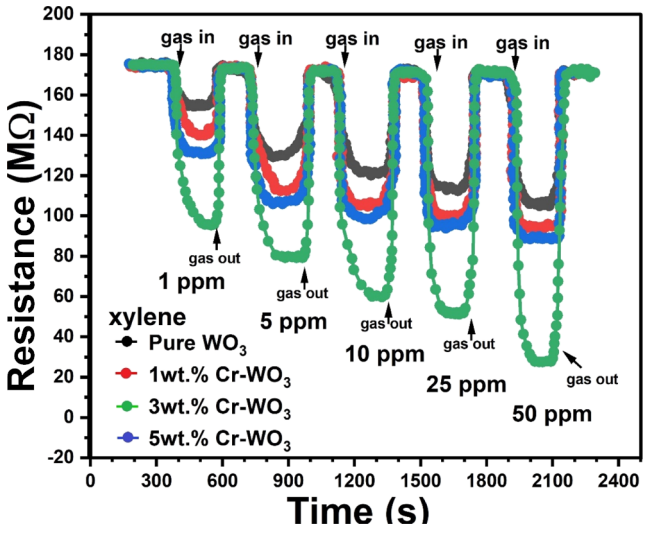

Figure 12. Dynamic response curve of the 3 wt % Cr-doped WO_3-based sensor.

$$C_8H_{10(g)} \rightarrow C_8H_{10(ads)} \quad (8)$$

$$C_8H_{10(ads)} + O^{\bullet-}_{2(ads)} \rightarrow C_8H_8O + H_2O + 2e^- \quad (9)$$

$$C_8H_8O + O^{\bullet-}_{2(ads)} \rightarrow CO_2 + H_2O + 2e^- \quad (10)$$

$$C_8H_{10(ads)} + 21O^{\bullet-}_{2\,(ads)} \leftrightarrow 8CO_{2\,(gas)} + 5H_2O_{(gas)} + 21e^- \quad (11)$$

As we know, the Cr-doped WO_3 film acts as an n-type semiconductor. If it is exposed to a reducing gas, such as xylene, the chemisorbed oxygen grasps the electron from the thin film surface and releases it into the conduction band. Hence, the potential barrier strength reduces as enhancing xylene exposure minimizes the film's resistance. Furthermore, when the target gas is removed from the chamber, adsorbed oxygen again captures electrons. This enhances the resistance and returns it to its original state, as shown in Figure 9.

Selectivity is defined as the ability of a sensor to discriminate interfering gases, and it is shown in Figure 10. To investigate the selectivity of these sensors, they are exposed to 50 ppm of several test gases at room temperature. The test gases include acetone, ammonia, ethanol, and xylene. The 3 wt % Cr-doped sensor responds significantly more to xylene than the other gases. It is due to the lower bond dissociation energy of xylene, and it can easily break its bonds to interact with the sensing material; subsequently, a considerable number of free electrons are released at the time of the reaction, which leads to a change in the resistance of the sensor element and a high sensitivity toward xylene.[39−41]

3.5.3. Transient Response Characteristics. The considerable variations in resistance caused by gas-particle adsorption and desorption on nanostructure surfaces affect the sensitivity of a chemical sensor. The time needed by the sensor to obtain 90% of its saturation resistance in the presence of the target gas is termed the response time, whereas the recovery time is explained as the time required by the sensor to attain 10% of the saturated resistance after the removal of the target gas. Transient response is one of the operational parameters describing a sensor's dynamics. The sensor has a fast response of 6.4 with a rapid response and recovery times of 12 and 7 s, respectively, toward 50 ppm of xylene at room temperature, and the transient response curve is shown in Figure 11. The dynamic response and recovery sensing aspects of the WO_3-based thin film varied with different concentrations of xylene in the range of 1 to 50 ppm at room temperature, as shown in Figure 12. When the sensor element is exposed to varying

Table 3. Comparison of Xylene Gas Sensing Properties of Several Other WO_3-Based Sensors

S.No	material	morphology	method	operating temperature (°C)	gas concentration (ppm)	response	response time (s)	recovery time (s)	ref
1	Ru-WO_3	nanosheet	hydrothermal and solvothermal	280	100	73			18
2	Au-WO_3	nanocubes	hydrothermal	255	10	26.4	1	1	19
3	Cr-WO_3	nanofiber	electrospinning method	255	100	35.4	1	2	20
4	WO_3	nanosheet	hydrothermal and sol-hydrothermal	320	50	36.27	23	19	21
5	CuO/WO_3	hierarchical structure	ultrasonic-wet chemical etching	260	50	6.36	5.5	16	22
6	Cr_2O_3/WO_3	hierarchical	water bath method	300	100	26	5	20	43
7	Pd-WO_3	nanoparticles	hydrothermal	230	10	21	1	2	44
8	Pt−Cr2O_3-WO_3	nanofibers	electrospinning	325	10	74.3	5	736	45
9	Cr-WO_3	nanoflakes	spray pyrolysis	RT	50	6.4	12	7	present work

https://doi.org/10.1021/acsomega.2c05589
ACS Omega 2022, 7, 47796−47805

concentrations of xylene, the resistance gradually decreases and tends to be smooth. This is consistent with the sensing properties of n-type semiconductor sensors.[42]

Table 3 compares the xylene gas-sensing performance of various WO_3-based sensors. The Table clearly shows that the 3 wt % Cr-doped WO_3 film has shown the best sensing characteristics at room temperature towards 50 ppm of xylene.

4. CONCLUSIONS

Undoped and Cr-doped WO_3 thin films are deposited using a simple and flexible spray pyrolysis technique, and the film's gas-sensing capabilities are systematically studied and reported. Structural investigations disclosed that the average crystallite size decreases and RMS surface roughness increases with increasing Cr doping concentration. The 3 wt % Cr-doped WO_3 sensor shows an excellent response toward xylene at room temperature among all these sensors. It has a high response of 6.4 with a fast response time of 12 s and a recovery time of 7 s toward 50 ppm of xylene. The gas-sensing characteristic of the sensing material is influenced by chemical components, nanoflake-like structures, and surface roughness. The Cr-doped WO_3 sensor's outstanding gas-sensing efficiency can be explained by the increase in surface morphology, roughness, and imperfections in WO_3-based nanostructures. The findings from this work confirmed that the Cr-doped WO_3 gas sensor could be a potential candidate to develop a low-cost xylene sensor operating under ambient conditions.

AUTHOR INFORMATION

Corresponding Authors

Saidi Reddy Parne − *Department of Applied Sciences, National Institute of Technology-Goa, Ponda 403401, India*; Email: psreddy@nitgoa.ac.in

Nagaraju Pothukanuri − *Nanosensor Research Laboratory, CMR Technical Campus, Hyderabad 501401, India; Sreenidhi University, Hyderabad, Telangana 501301, India*; orcid.org/0000-0003-1894-6825; Email: nagarajuphysics@gmail.com

Authors

Srinivasa Rao Sriram − *Department of Applied Sciences, National Institute of Technology-Goa, Ponda 403401, India*

Dhananjay Joshi − *Department of Physics, Indian Institute of Science Education and Research Mohali, Mohali 140306, India*

Damodar Reddy Edla − *Department of Computer Science, National Institute of Technology-Goa, Ponda 403401, India*

Complete contact information is available at: https://pubs.acs.org/10.1021/acsomega.2c05589

Notes

The authors declare no competing financial interest.

ACKNOWLEDGMENTS

Dr. P. Nagaraju would like to express his gratitude to UGC-DAE-CSR, Indore, for providing experimental facilities under the CSR−I.C.−MSRSR-21/CRS-229/2017−18/1310 project. He also thanks Sri. Ch. Gopal Reddy, Chairman, and Dr. A. Rajireddy, Director, CMR Technical Campus, for their encouragement to complete the present work. The authors would like to thank Dr. E. Senthamarai Kannan, Department of Physics, and Kumar Kanneboyena, Central Sophisticated Instrumentation Facility, BITS-Pilani KK Birla Goa Campus, for providing field emission scanning electron microscopy measurements.

REFERENCES

(1) Chen, K.; Zhou, Y.; Jin, R.; Wang, T.; Liu, F.; Wang, C.; Yan, X.; Sun, P.; Lu, G. Gas sensor based on cobalt-doped 3D inverse opal SnO_2 for air quality monitoring. *Sens. Actuators, B* **2022**, *350*, 130807.

(2) Tancev, G.; Toro, F. G. Variational Bayesian calibration of low-cost gas sensor systems in air quality monitoring. *Measurement: Sensors.* **2022**, *19*, 100365.

(3) Seesaard, T.; Goel, N.; Kumar, M.; Wongchoosuk, C. Advances in gas sensors and electronic nose technologies for agricultural cycle applications. *Comput. Electron. Agric.* **2022**, *193*, 106673.

(4) Wijaya, D. R.; Afianti, F.; Arifianto, A.; Rahmawati, D.; Kodogiannis, V. S. Ensemble machine learning approach for electronic nose signal processing. *Sens. Bio-Sens. Res.* **2022**, *36*, 100495.

(5) Yan, M. R.; Hsieh, S.; Ricacho, N. Innovative Food Packaging, Food Quality and Safety, and Consumer Perspectives. *Processes* **2022**, *10*, 747.

(6) Saeed, R.; Feng, H.; Wang, X.; Zhang, X.; Fu, Z. Fish quality evaluation by sensor and machine learning: A mechanistic review. *Food Control* **2022**, *137*, 108902.

(7) Wasilewski, T.; Brito, N. F.; Szulczyński, B.; Wojciechowski, M.; Buda, N.; Melo, A. C. A.; Kamysz, W.; Gębicki, J. Olfactory receptor-based biosensors as potential future tools in medical diagnosis. *TrAC, Trends Anal. Chem.* **2022**, *150*, 116599.

(8) Korotcenkov, G.; Brinzari, V.; Ham, M. H. Materials acceptable for gas sensor design: advantages and limitations. *Key Eng. Mater.* **2018**, *780*, 80−89.

(9) Epifani, M. Mechanistic Insights into WO_3 Sensing and Related Perspectives. *Sensors* **2022**, *22*, 2247.

(10) Sriram, S. R.; Parne, S.; Vaddadi, V. S. C. S.; Edla, D.; Nagaraju, P.; Avala, R. R.; Yelsani, V.; Sontu, U. B. Nanostructured WO_3 based gas sensors: a short review. *Sens. Rev.* **2021**, *41*, 406−424.

(11) Kodam, P. M.; Ghadage, P. A.; Nadargi, D. Y.; Shinde, K. P.; Mulla, I.-S.; Park, J.-S.; Suryavanshi, S. S. Ru, Pd doped WO_3 nanomaterials: A synergistic effect of noble metals to enhance the acetone response properties. *Ceram. Int.* **2022**, *48*, 17923−17933.

(12) Punginsang, M.; Zappa, D.; Comini, E.; Wisitsoraat, A.; Sberveglieri, G.; Ponzoni, A.; Liewhiran, C. Selective H_2S gas sensors based on ohmic hetero-interface of Au-functionalized WO_3 nanowires. *Appl. Surf. Sci.* **2022**, *571*, 151262.

(13) Mathankumar, G.; Bharathi, P.; M, M. M.; Archana, J.; Harish, S.; Navaneethan, M. Defect manipulation of WO_3 nanostructures by yttrium for ultra-sensitive and highly selective NO_2 detection. *Sens. Actuators, B* **2022**, *353*, 131057.

(14) Chakraborty, N.; Mondal, S. Dopant-mediated surface charge imbalance for enhancing the performance of metal oxide chemiresistive gas sensors. *J. Mater. Chem. C* **2022**, *10*, 1968−1976.

(15) Varudkar, H. A.; Umadevi, G.; Nagaraju, P.; Dargad, J. S.; Mote, V. D. Fabrication of Al-doped ZnO nanoparticles and their application as a semiconductor-based gas sensor for the detection of ammonia. *J. Mater. Sci. Mater. Electron.* **2020**, *31*, 12579−12585.

(16) Nagaraju, P.; Vijayakumar, Y.; Choudhary, R. J.; Ramana Reddy, M. V. Preparation and characterization of nanostructured Gd doped cerium oxide thin films by pulsed laser deposition for acetone sensor application. *J. Mater. Sci. Eng. B* **2017**, *226*, 99−106.

(17) Anusha; Ani, A.; Poornesh, P.; Antony, A.; Bhaghyesh; Shchetinin, V.; Nagaraja, K. K.; Chattopadhyay, S.; Vinayakumar, K. B. Impact of Ag on the Limit of Detection towards NH_3-Sensing in Spray-Coated WO_3 Thin-Films. *Sensors* **2022**, *22*, 2033.

(18) Wang, C.; Zhang, S.; Qiu, L.; Rasaki, S. A.; Qu, F.; Thomas, T.; Liu, Y.; Yang, M. Ru-decorated WO_3 nanosheets for efficient xylene gas sensing application. *J. Alloys Compd.* **2020**, *826*, 154196.

(19) Li, F.; Guo, S.; Shen, J. L.; Shen, D.; Sun, B.; Wang, Y.; Chen, S.; Ruan, S. Xylene gas sensor based on Au-loaded $WO_3{\cdot}H_2O$

https://doi.org/10.1021/acsomega.2c05589
ACS Omega 2022, 7, 47796−47805

nanocubes with enhanced sensing performance. *Sens. Actuators, B* **2017**, *238*, 364−373.
(20) Li, F.; Ruan, S.; Zhang, N.; Yin, Y.; Guo, S.; Chen, Y.; Zhang, H.; Li, C. Chemical Synthesis and characterization of Cr-doped WO_3 nanofibers for conductometric sensors with high xylene sensitivity. *Sens. Actuators, B* **2018**, *265*, 355−364.
(21) Zhang, D.; Fan, Y.; Li, G.; Ma, Z.; Wang, X.; Cheng, Z.; Xu, J. Highly sensitive BTEX sensors based on hexagonal WO_3 nanosheets. *Sens. Actuators, B* **2019**, *293*, 23−30.
(22) Guo, M.; Luo, N.; Chen, Y.; Fan, Y.; Wang, X.; Xu, J. Fast-response MEMS xylene gas sensor based on CuO/WO_3 hierarchical structure. *J. Hazard. Mater.* **2022**, *429*, 127471.
(23) Sriram, S. R.; Parne, S. R.; Pothukanuri, N.; Edla, D. R. Prospects of spray pyrolysis technique for gas sensor applications—A comprehensive review. *J. Anal. Appl. Pyrolysis* **2022**, *164*, 105527.
(24) Dalenjan, F. A.; Bagheri−Mohagheghi, M. M.; Shirpay, A. The effect of cobalt (Co) concentration on structural, optical, and electrochemical properties of tungsten oxide (WO_3) thin films deposited by spray pyrolysis. *J. Solid State Electrochem.* **2022**, *26*, 401−408.
(25) Acosta, D.; Hernández, F.; López-Suárez, A.; Magaña, C. WO_3:Mo and WO_3:Ti thin films deposited by spray pyrolysis: The influence of metallic concentration on physical properties: An electron microscopy and atomic force study. *Solid State Phenom.* **2019**, *286*, 49−63.
(26) Upadhyay, S. B.; Mishra, R. K.; Sahay, P. P. Cr-doped WO_3 nanosheets: Structural, optical and formaldehyde sensing properties. *Ceram. Int.* **2016**, *42*, 15301−15310.
(27) Nagaraju, P.; VijayaKumar, Y.; Radhika, P.; Choudhary, R. J.; RamanaReddy, M. V. Structural, morphological, optical and gas sensing properties of nanocrystalline ceria thin films. *Mater. Today Proc.* **2016**, *3*, 4009−4018.
(28) Nagaraju, P.; VijayaKumar, Y.; Radhika, P.; Choudhary, R. J.; RamanaReddy, M. V. Structural, morphological, optical and gas sensing properties of nanocrystalline ceria thin films. *Mater. Today Proc.* **2016**, *3*, 4009−4018.
(29) Godavarti, U. D.; Nagaraju, P.; Yelsani, Y.; Pushukuri, P.; Reddy, P. S.; Dasari, D. Synthesis and characterization of ZnS-based quantum dots to trace low concentration of ammonia. *J. Semiconduct.* **2021**, *42*, 122901.
(30) Filipovic, L.; Selberherr, S. Performance and Stress Analysis of Metal Oxide Films for CMOS-Integrated Gas Sensors. *Sensors* **2015**, *15*, 7206−7227.
(31) Dasari, S. G.; Nagaraju, P.; Yelsani, V.; Tirumala, S.; Ramana Reddy, M. V. Nanostructured Indium Oxide Thin Films as a Room Temperature Toluene Sensor. *ACS Omega* **2021**, *6*, 17442−17454.
(32) Bhat, P.; Naveen Kumar, S. K.; Nagaraju, P. Synthesis and characterization of ZnO-MWCNT nanocomposites for 1- butanol sensing application at room temperature. *Phys. B* **2019**, *570*, 139−147.
(33) Mohan, L.; Avani, A. V.; Kathirvel, P.; Marnadu, R.; Packiaraj, R.; Joshua, J. R.; Nallamuthu, N.; Shkir, M.; Saravanakumar, S. Investigation on structural, morphological and electrochemical properties of Mn doped WO_3 nanoparticles synthesized by co-precipitation method for supercapacitor applications. *J. Alloys Compd.* **2021**, *882*, 160670.
(34) Gouadec, G.; Colomban, P. Raman Spectroscopy of nanomaterials: How spectra relate to disorder, particle size and mechanical properties. *Prog. Cryst. Growth Charact. Mater.* **2007**, *53*, 1−56.
(35) Gavaskar, D. S.; Nagaraju, P.; Vijayakumar, Y.; Reddy, P. S.; Ramana Reddy, M. V. Low-cost ultra-sensitive SnO_2-based ammonia sensor synthesized by hydrothermal method. *J. Asian Ceram. Soc.* **2020**, *8*, 605−614.
(36) Ghasemi, F.; Ghasemi, M.; Eftekhari, L.; Soleimanian, V. Comparison and influence of metal dopants on the opto-electrical, microstructure and gas sensing properties of nanostructured indium oxide films. *Opt Laser. Technol.* **2022**, *146*, 107564.
(37) Tudose, I. V.; Horváth, P.; Suchea, M.; Christoulakis, S.; Kitsopoulos, T.; Kiriakidis, G. Correlation of ZnO thin film surface properties with conductivity. *J. Appl. Phys.* **2007**, *89*, 57−61.
(38) Manjunath, G.; Nagaraju, P.; Mandal, M. A comparative study on enhancer and inhibitor of glycine−nitrate combustion ZnO screen-printed sensor: detection of low concentration ammonia at room temperature. *J. Mater. Sci. Mater. Electron.* **2020**, *31*, 10366−10380.
(39) Dean, J. A.; *Handbook of Chemistry*; 15th ed.; McGraw Hill Inc.: New York, NY, 1999.
(40) Nagaraju, P.; Vijayakumar, Y.; Ramana Reddy, M. V. Room-temperature BTEX sensing characterization of nanostructured ZnO thin films. *J. Asian Ceram. Soc.* **2019**, *7*, 141−146.
(41) Wang, L.; Li, Y.; Yue, W.; Gao, S.; Zhang, C.; Chen, Z. High-Performance Formaldehyde Gas Sensor Based on Cu-doped Sn_3O_4, Hierarchical Nanoflowers. *IEEE Sens. J.* **2020**, *20*, 6945−6953.
(42) Wu, H.; Zhou, Y.; Guo, J.; Zhao, L.; Wang, T.; Yan, X.; Wang, C.; Liu, F.; Sun, P.; Lu, G. Highly sensitive and selective xylene sensor based on p-p heterojunctions composites derived from off-stoichiometric cobalt tungstate. *Sens. Actuators, B* **2022**, *351*, 130973.
(43) Li, Y.; Li, F.; Li, C.; Wei, W.; Jiang, D.; Zhu, L.; Sun, D.; Zhang, X.; Ruan, S. The preparation of Cr_2O_3@WO_3 hierarchical nanostructures and their application in the detection of volatile organic compounds (VOCs). *RSC Adv.* **2015**, *5*, 61528−61534.
(44) Li, F.; Qin, Q.; Zhang, N.; Chen, C.; Sun, L.; Liu, X.; Chen, Y.; Li, C.; Ruan, S. Improved gas sensing performance with Pd-doped WO_3·H_2O nanomaterials for the detection of xylene. *Sens. Actuators, B* **2017**, *244*, 837−848.
(45) Feng, C.; Jiang, Z.; Wu, J.; Chen, B.; Lu, G.; Huang, C. Pt-Cr_2O_3-WO_3 composite nanofibers as gas sensors for ultra-high sensitive and selective xylene detection. *Sens. Actuators, B* **2019**, *300*, 127008.

https://doi.org/10.1021/acsomega.2c05589
ACS Omega 2022, 7, 47796−47805